2007 IEEE International Conference on
Robotics and Automation
Roma, Italy, 10-14 April 2007

Development of a Novel 3-DoF Purely Translational Parallel Mechanism

Yunjiang Lou, Jiangang Li, Jinbo Shi, and Zexiang Li

***Abstract*— In view of the successful application of planar parallelogram in the Delta robot and its variants, we are interested to investigate mechanisms consisting of spatial parallelograms. The spatial parallelogram, denoted by P_a^*, is a 2-SS (S stands for a spherical joint) parallel mechanism having identical length for opposite links. We show that a 3-PP_a^* mechanism is generically undergoes 3-dimensional purely translational motion. Based on the 3-PP_a^* topology, an integrated optimal design on both architecture and geometry design is carried out. Using the formulation of maximizing effective cubic workspace, the Orthopod, which has three orthogonally arranged linear joint axes, is found to be the best in our settings. A prototype machine of the Orthopod is thus designed and manufactured.**

***Index Terms*— parallel mechanism, pure translation, optimal design.**

I. INTRODUCTION

Most existing parallel kinematic machines are based on the 6-DoF Gough-Stewart platform architecture [1][2]. However, six degrees of freedom are often superfluous for machine tools and other applications. In addition, 6-DoF parallel manipulators suffer from the disadvantages of difficult forward kinematics, coupled position and orientation, and small workspace. To overcome the above shortcomings, parallel manipulators with 3-DoF have been investigated for relevant applications. Typical representatives for 3-DoF purely translational parallel mechanisms are (a) the Delta robot invented by Clavel [3] and its variants, e.g., the Orthoglide proposed by Chablat and Wenger [4], and (b) the 3-UPU parallel manipulator first proposed by Tsai [5] and later generalized by Di Gregorio and Parenti-Castelli [6].

In view of the successful application of planar parallelogram in the Delta robot and its variants, we investigate its spatial counterpart, the spatial parallelogram P_a^*. Here, P_a^* is in fact a 2-SS parallel mechanism with identical opposite links. In this paper, a subchain having PP_a^* topology, i.e., a serial connection of a prismatic joint and a P_a^*, see Fig. 1, is proposed to serve as a leg of a parallel mechanism. The subchain consists of 4 passive joints. A computation in section II shows that the PP_a^* subchain undergoes 5-DoF motion. Hence, the PP_a^* subchain is non-overconstrained, while the Delta robot has three identical over-constrained subchains. For the Delta type robots, deviations in manufacturing will make it difficult to assemble parts into a whole machine since there are superfluous mobility constraints. We can show that a parallel mechanism consisting of 3 PP_a^* subchains generically undergoes 3-DoF purely translational motion. For the engraving machine application, it is essential to gain rapid dynamic response. The base fixed prismatic joints are therefore taken as actuated joints to make moving part of a mechanism as light as possible. A prototype machine was designed and manufactured accordingly.

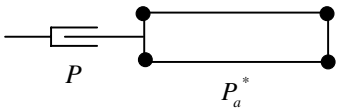

Fig. 1. A schematic of PP_a^* subchain

The paper is organized as follows. In section II, mobility analysis of a 3-PP_a^* parallel mechanism is presented using the theory of Lie algebra. Tangent spaces of a spatial parallelogram, a PP_a^* subchain, and a 3-PP_a^* parallel mechanism respective at their home configurations are computed. In section III, an optimal design including both architecture and geometry parameters is conducted. It is shown that the Orthopod, which has mutually perpendicular fixed prismatic joint axes, possesses the largest effective cubic workspace given a constraint on overall size of the mechanism. A prototype machine of the Orthopod is thus designed and manufactured. Finally, a conclusion is drawn in section IV.

II. MOBILITY ANALYSIS

In this section, we analyze mobility of a 3-PP_a^* parallel mechanism. By computing tangent space of its configuration space at some point, it is concluded that the 3-PP_a^* parallel mechanism undergoes 3-DoF purely translation generically.

A. Tangent Space of the Spatial Parallelogram

Let us first investigate mobility of the spatial parallelogram P_a^* as shown in Fig.2. As well known, a spherical joint is equivalent to a serial connection of three revolute joints, whose axes ω_i, $i = 1, \cdots, 3$ intersect at a common point perpendicularly. We assume that ω_i, $i = 1, \cdots, 3$ observes the right-hand rule for convenience.

Let us denote the configuration spaces of a P_a^* and its i-th subchain by C_M and C_{M_i}, respectively. From Fig. 2-(b), we have $q_{i2} = q_{i1} + \mathbf{v}$. The *home position* of a PP_a^*

This project is supported by RGC Grant No. HKUST 6301/03E, HKUST 6301/04E and 616805, and in part by NSFC grants No.50505009 and 50535010.

Yunjiang Lou is with the Division of Control and Mechatronics (CoME), Harbin Institute of Technology (HIT) Shenzhen Graduate School (SZGS), Shenzhen, China, and is now a research staff of Dept. Electronic and Computer Engineering (ECE), the Hong Kong University of Science and Technology (HKUST), Clear Water Bay, Kowloon, Hong Kong SAR. (louyj@hitsz.edu.cn)

Jiangang Li is a Postdoctoral researcher of the CoME Division, HIT SZGS, Shenzhen, China (Jiangang_lee@163.com)

Jinbo Shi is a Mphil student of the CoME Division, HIT SZGS, Shenzhen, China (shijinbo@hitsz.edu.cn)

Zexiang Li is with the Dept. of ECE, HKUST, and the CoME Division of HIT SZGS, (eezxli@ee.ust.hk)

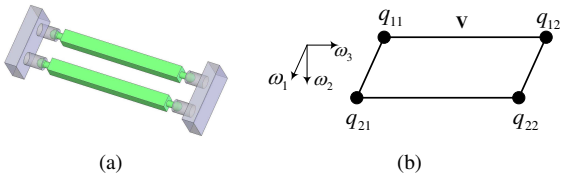

(a) (b)

Fig. 2. (a) A CAD model of the spatial parallelogram; (b) A schematic of the spatial parallelogram.

subchain is taken as the configuration where P_a^* keeps rectangular and the axis of P joint is parallel to $\mathbf{v}$. At the home configuration e, the spatial velocity spaces $T_eC_{M_i}$ for the two legs M_i, $i = 1, 2$, are given as follows.

$$T_eC_{M_i} = \text{span}\{\begin{bmatrix} q_{i1} \times \omega_1 \\ \omega_1 \end{bmatrix}, \begin{bmatrix} q_{i1} \times \omega_2 \\ \omega_2 \end{bmatrix}, \begin{bmatrix} q_{i1} \times \omega_3 \\ \omega_3 \end{bmatrix}, \begin{bmatrix} q_{i2} \times \omega_1 \\ \omega_1 \end{bmatrix}, \begin{bmatrix} q_{i2} \times \omega_2 \\ \omega_2 \end{bmatrix}, \begin{bmatrix} q_{i2} \times \omega_3 \\ \omega_3 \end{bmatrix}\}$$

Assume $q_{i1} = \alpha_i\omega_1 + \beta_i\omega_2 + \gamma_i\omega_3,\ i = 1, 2$, where α_i, β_i, and γ_i are all constant scalars, by some manipulations, we have

$$T_eC_{M_i} = \text{span}\{\begin{bmatrix} -\beta_i\omega_3 \\ \omega_1 \end{bmatrix}, \begin{bmatrix} \alpha_i\omega_3 \\ \omega_2 \end{bmatrix}, \begin{bmatrix} 0 \\ \omega_3 \end{bmatrix}, \begin{bmatrix} \omega_1 \\ 0 \end{bmatrix}, \begin{bmatrix} \omega_2 \\ 0 \end{bmatrix}\}.$$

In order to obtain a concise expression, we move the coordinate frame such that its origin coincides q_{11}. This loses no generality and leads to $q_{11} = (\alpha_1, \beta_1, \gamma_1) = (0, 0, 0)$ and $q_{21} = (\alpha_2, \beta_2, \gamma_2) = (\alpha_2, 0, 0)$ with $\alpha_2 \neq 0$ when $q_{11} \neq q_{21}$. The intersection of the two velocity subspaces gives

$$T_eC_{M_1} \cap T_eC_{M_2} = \text{span}\{\begin{bmatrix} 0 \\ \omega_1 \end{bmatrix}, \begin{bmatrix} 0 \\ \omega_3 \end{bmatrix}, \begin{bmatrix} \omega_1 \\ 0 \end{bmatrix}, \begin{bmatrix} \omega_2 \\ 0 \end{bmatrix}\}.$$

Therefore, the spatial parallelogram conducts a 4-DoF motion instantaneously at the home position, more precisely, two DoF translation along ω_1-ω_2 plane, and two DoF rotation about ω_1-axis and ω_3-axis, respectively. The expression (1) is precisely the tangent space of C_M at e.

B. Tangent Space of the 3-PP_a^* Parallel Mechanism

Let us denote the axis of the P joint in Fig. 1 by $\mathbf{e}$. Therefore, there exist constant real numbers a, b, c such that $\mathbf{e} := a\omega_1 + b\omega_2 + c\omega_3$. When $c \neq 0$, with notation C being the configuration space of a PP_a^* subchain, we have

$$\begin{aligned} T_eC &= T_eC_M \bigcup T_eP \\ &= \text{span}\{\begin{bmatrix} 0 \\ \omega_1 \end{bmatrix}, \begin{bmatrix} 0 \\ \omega_3 \end{bmatrix}, \begin{bmatrix} \omega_1 \\ 0 \end{bmatrix}, \begin{bmatrix} \omega_2 \\ 0 \end{bmatrix}, \begin{bmatrix} \omega_3 \\ 0 \end{bmatrix}\}. \end{aligned}$$

Note, when $c = 0$, i.e., the P joint axis is in ω_1-ω_2 plane, T_eC reduces to the tangent space of the P_a^*.

Let us consider a parallel mechanism consisting of three PP_a^* subchains whose axes are $(\omega_1^i, \omega_2^i, \omega_3^i)$, $i = 1, \cdots, 3$. The tangent spaces of the three PP_a^* subchains are given by $T_eC_i = R_i \times T_i$, $i = 1, \cdots, 3$, where R_i and T_i are respectively velocity spaces due to rotation and translation,

$$\begin{aligned} R_i &= \text{span}\{\begin{bmatrix} 0 \\ \omega_1^i \end{bmatrix}, \begin{bmatrix} 0 \\ \omega_3^i \end{bmatrix}\}; \\ T_i &= \text{span}\{\begin{bmatrix} \omega_1^i \\ 0 \end{bmatrix}, \begin{bmatrix} \omega_2^i \\ 0 \end{bmatrix}, \begin{bmatrix} \omega_3^i \\ 0 \end{bmatrix}\}. \end{aligned}$$

The tangent space of the parallel mechanism T_eC_S is the intersection of tangent spaces of the three PP_a^* subchains as follows.

$$T_eC_S = \cap_{i=1}^3 T_eC_i = \cap_{i=1}^3 R_i \times \cap_{i=1}^3 T_i \tag{1}$$

Clearly, each T_i is a velocity space of purely translational motion at e and $T_i = T_j$, for $i, j = 1, \cdots, 3$. Assume that x, y, z are respectively directions of x-, y-, z-axis for an arbitrary spatial frame, we have

$$\cap_{i=1}^3 T_i = T_i = \text{span}\{\begin{bmatrix} x \\ 0 \end{bmatrix}, \begin{bmatrix} y \\ 0 \end{bmatrix}, \begin{bmatrix} z \\ 0 \end{bmatrix}\}. \tag{2}$$

Given a generic arrangement of axes that any two of ω_3^i, $i = 1, \cdots, 3$ are *not* parallel, i.e., $\omega_3^i \neq \omega_3^j$, $i \neq j$ and $i, j = 1, \cdots, 3$, we have $\cap_{i=1}^3 R_i = \{I\}$. Therefore, the tangent space of the parallel mechanism at the home position T_eC_S is computed as following.

$$T_eC_S = \cap_{i=1}^3 T_eC_i = \text{span}\{\begin{bmatrix} x \\ 0 \end{bmatrix}, \begin{bmatrix} y \\ 0 \end{bmatrix}, \begin{bmatrix} z \\ 0 \end{bmatrix}\} \tag{3}$$

The expression (3) shows that the parallel mechanism consisting of 3 PP_a^* subchains generally conducts a 3-DoF purely translational motion instantaneously at home position.

Remark *1:* It can be easily verified that a parallel mechanism consisting of more than 3 PP_a^* subchains still undergoes a 3-DoF purely translational motion instantaneously at home position. Furthermore, for a spatial parallelogram having 3-SS topology (denote by $P_a^{\#}$), it undergoes 3-DoF motion instantaneously at home position, two DoF translational motion along $\omega_1\omega_2$ plane and one rotational DoF about ω_3, see [7]. Let us consider a subchain consisting of a prismatic joint and a $P_a^{\#}$. We can show that a parallel mechanism consisting of 2 or more such subchains results in 3-DoF purely translational motion instantaneously at home position.

C. Motion Type of the 3-PP_a^* Parallel Mechanism

Next we'll show a 3-PP_a^* parallel mechanism indeed undergoes 3-DoF purely translational motion in a finite neighborhood of the home configuration by introducing the following proposition.

Proposition *1:* Given a fully parallel manipulator $\mathcal{M}$, which is a parallel connection of k subchains, $\mathcal{M}_1, \cdots, \mathcal{M}_k$. We denotes the configuration space of each subchain by C_i, $i = 1, \cdots, k$. Suppose that each C_i contains a set Q_u, which is a connected open subset of Q around e. Here $Q \subset SE(3)$ is a submanifold.

$$Q_u \subseteq C_i, i = 1, \cdots, k \tag{4}$$

and consequently $Q_u \subseteq C$, where C is the configuration space of $\mathcal{M}$. If the condition

$$T_eQ = T_eC_1 \cap \cdots \cap T_eC_k \tag{5}$$

holds, C agrees with Q at Q_u, the neighborhood of e. □

Readers are referred to [8][9] for detailed proof of the proposition. The proposition provides us a tool to analyze parallel mechanisms. When we encounter a parallel mechanism, we first compute the tangent space of the mechanism at the home position (or other typical configuration). If all subchains contain a finite motion and the parallel mechanism has the same tangent space as that of the finite motion at the home position (or other typical configuration), then the parallel mechanism undergoes the motion type corresponding to the finite motion. In our case, we have computed tangent space of the 3-PP_a^* parallel mechanism at home position. Next we need to investigate the motion of each subchain.

By observation, easy to find that the motion of a spatial parallelogram contains the one generated by a U^* joint, which is a parallel connection of three UU legs [10]. As we know, a U^* joint undergoes 2-DoF spherically translational motion perpendicular to its axis [8]. A P_a^* must contain finite 2-DoF translation motion since it has less restriction than U^*. Therefore, each PP_a^* subchain, a serial connection of a prismatic joint and a spatial parallelogram, must contain a finite 3-DoF translational motion. By the Proposition 1 and the tangent space of the mechanism at home position (3), we conclude that the 3-PP_a^* parallel mechanism undergoes finite 3-DoF purely translational motion.

III. Optimal Design of the 3-PP_a^* Parallel Mechanism

In this section, we will determine architecture for a parallel mechanism having 3-PP_a^* topology as discussed above. Basically, there are three primary stages in design of a parallel mechanism, say topology, architecture, and geometry design. The *topology design* or type synthesis is to determine number of subchains and joint types and connections in each subchain such that the resulting mechanism is able to undergo some given (finite) motion. Based on the chosen topology, *architecture design* is to determine axes of fixed joints and their relative arrangement. After topology design and architecture design, *geometry design* is to determine size issue of the decided architecture, e.g., the link lengths and the size of the base/the end-effector. Note sometimes people do not discriminate between concepts of architecture and geometry design and term them together as geometry (architecture, dimension) design. In this paper, the defined concepts of architecture and geometry design are used.

In design of a parallel mechanism, most optimal designs actually do the job of geometry design only [11][4][12][13]. People usually first come up an topology and architecture by their *experience* and *intuition* and then do the geometry design job by formulating the design problem as an optimization problem and searching the optimal geometric parameters for the architecture. As well known, performance

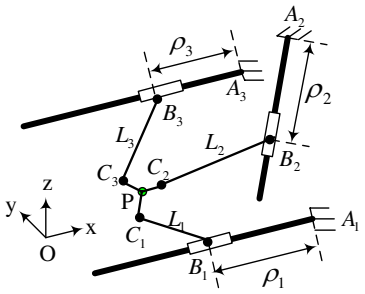

Fig. 3. A schematic of the 3-PP_a^* parallel mechanism

of a parallel mechanism depends not only on its geometry, but also on its architecture and topology. In fact, the resulting mechanism may be optimal for the chosen architecture only. It is usually not the best among the mechanisms having a common topology.

In the last section, we have shown that the parallel mechanism having 3-PP_a^* topology undergoes 3-DoF purely translation. There are infinite number of architectures that realize the topology. Usually we cannot determine which architecture is the best in some performance by simply our intuition and experience. Therefore, it is necessary to include both architecture and geometry parameters when optimally designing a parallel mechanism. Hence, Our problem is, *given the 3-PP_a^* topology, to determine both its architecture and geometry such that the resulting mechanism reaches best performance.*

A. Kinematic Analysis

Let us consider a general architecture for the 3-PP_a^* parallel mechanism as shown in Fig. 3. Here, A_i is the fixed footprint where the i-th subchain connects, B_i represents position of the slider on the i-th linear actuator, C_i is the point on the end-effector to which the i-th spatial parallelogram is attached, and P is the reference point on the end-effector. By setting up a fixed Cartesian coordinate frame, loop closure equations can be readily derived. Let $\mathbf{p} = \overrightarrow{OP}$, $\mathbf{a}_i = \overrightarrow{OA_i}$, $\mathbf{c}_i = \overrightarrow{C_iP}$, $\mathbf{e}_i = \frac{\overrightarrow{A_iB_i}}{\|\overrightarrow{A_iB_i}\|}$ the direction of linear actuation, $\mathbf{w}_i = \frac{\overrightarrow{B_iC_i}}{\|\overrightarrow{B_iC_i}\|}$, the direction of the spatial parallelogram, $\rho_i = \|\overrightarrow{A_iB_i}\|$ the length of i-th linear joint, and $L_i = \|\overrightarrow{B_iC_i}\|$ the length of spatial parallelogram, we have

$$\mathbf{a}_i + \rho_i\mathbf{e}_i + L_i\mathbf{w}_i + \mathbf{c}_i = \mathbf{p}, \quad i = 1, \cdots, 3.$$

Clearly, $\mathbf{a}_i$ and $\mathbf{c}_i$ are both constant and they have combined effect on kinematics via their sum $\mathbf{a}_i + \mathbf{c}_i$. Therefore, we need only to consider their sum and define $\mathbf{d}_i := \mathbf{a}_i + \mathbf{c}_i$. The loop closure equations become

$$\mathbf{d}_i + \rho_i\mathbf{e}_i + L_i\mathbf{w}_i = \mathbf{p}, \quad i = 1, \cdots, 3. \tag{6}$$

Given Cartesian position $\mathbf{p}$, taking norm of both sides of (6) we can solve for the inverse kinematics as follows.

$$\rho_i = (\mathbf{p} - \mathbf{d}_i)^T\mathbf{e}_i - \sqrt{[(\mathbf{p} - \mathbf{d}_i)^T\mathbf{e}_i]^2 - \|\mathbf{p} - \mathbf{d}_i\|^2 + L_i^2} \tag{7}$$

This leads to

$$\mathbf{w}_i = \frac{\mathbf{p} - \mathbf{d}_i - \rho_i \mathbf{e}_i}{L_i}. \tag{8}$$

Differentiating (6) with respect to time t leads to

$$\dot{\mathbf{p}} = \dot{\rho}_i \mathbf{e}_i + L_i \dot{\mathbf{w}}_i, \quad i = 1, \cdots, 3.$$

Dot-multiplying $\mathbf{w}_i$ on both sides of the above equations and stacking them in matrix form, we obtain the instantaneous velocity map relating the Cartesian velocity $\dot{\mathbf{p}}$ and the joint velocity $\dot{\rho}$ as follows.

$$J_\rho \dot{\rho} = J_x \dot{X}, \tag{9}$$

where $\dot{X} = \dot{\mathbf{p}} = [\dot{x}, \dot{y}, \dot{z}]^T$, $\dot{\rho} = [\dot{\rho}_1, \dot{\rho}_2, \dot{\rho}_3]^T$ and

$$J_\rho = \begin{bmatrix} \mathbf{w}_1^T \mathbf{e}_1 & 0 & 0 \\ 0 & \mathbf{w}_2^T \mathbf{e}_2 & 0 \\ 0 & 0 & \mathbf{w}_3^T \mathbf{e}_3 \end{bmatrix}, \qquad J_x = \begin{bmatrix} \mathbf{w}_1^T \\ \mathbf{w}_2^T \\ \mathbf{w}_3^T \end{bmatrix}.$$

Therefore, when J_ρ is nonsingular, we obtain $\dot{\rho} = J\dot{X}$ with $J = J_\rho^{-1} J_x$.

In order to fully decide architecture and geometry of a 3-PP_a^* parallel mechanism, we need to determine values of

1) the position of footprints A_i, $\mathbf{a}_i$;
2) axes of base attached prismatic joints $\mathbf{e}_i$;
3) geometric parameters L_i and $\mathbf{c}_i$.

According to above kinematic analysis, instead of considering $\mathbf{a}_i$ and $\mathbf{c}_i$ independently, we investigate kinematic effects of their sum $\mathbf{d}_i$. Therefore, we need to determine values of $\mathbf{d}_i$, $\mathbf{e}_i$, and L_i, $i = 1, \cdots, 3$. In practical implementation, we use the same geometry for all three subchains, i.e., $L_i = L$, $i =, 1, \cdots, 3$ for manufacturing reason.

B. Optimal Architecture and Geometry Design of the 3-PP_a^* Mechanism

Next we will optimally design the 3-PP_a^* parallel mechanism using the formulation discussed in [14]. The target is to obtain the best mechanism that maximizes effective regular workspace under size constraints. The world frame is set up with its origin coinciding with the reference point P at home position.

- *Objective*: A cube with side length $2l$ in $\mathbb{R}^3$ is designated as its (translational) workspace W. The objective function is chosen as $\Phi = l$ to characterize the volume of W. The center of the maximal cubic workspace is taken as $[x_c, y_c, z_c]^T$, which is undetermined.
- *Constraints on mechanism size*: A constraint on the manipulator size is imposed by normalizing length of its subchain

  $$\rho_{max} + L = 1,$$

  where ρ_{max} is the stroke of each prismatic joint.
- *Constraints on dexterity*: Let us define dexterity measure as $\kappa(J) = \sigma_{\min}(J)/\sigma_{\max}(J)$, a dexterity constraint is imposed with $\gamma = 0.2$,

  $$\kappa(J) \geq \gamma.$$

- *Constraints due to actuated joint limits*: As discussed in [14], all inverse kinematic solutions should be in the given actuation range $[0, \rho_{max}]$, i.e., the actuation length ρ_i is constrained by

  $$0 \leq \rho_i(X, \alpha) \leq \rho_{max}, \quad i = 1, \cdots, 3.$$

- *Constraints due to passive joint limits:* Assume the ball joint range is $[0, \mathcal{B}]$, the constraints due to ball joint limits are given as follows.

  $$0 \leq \text{Angle}(\mathbf{w}_j, \mathbf{w}_j^0) \leq \mathcal{B}, \quad j = 1, \cdots, 3.$$

  where $\mathbf{w}_j^0$ is the direction of spatial parallelogram at home configuration. $\text{Angle}(\mathbf{w}_j, \mathbf{w}_j^0)$ measures the angle between vectors $\mathbf{w}_j$ and $\mathbf{w}_j^0$. We take $\mathcal{B} = 30^\text{o}$ in the simulation.
- The set of design parameters is determined, $\alpha = (\mathbf{d}_1, \mathbf{d}_2, \mathbf{d}_3, \mathbf{e}_1, \mathbf{e}_2, \mathbf{e}_3, L, x_c, y_c, z_c)$. However, there are three constraint equations for home position requirement, $\mathbf{d}_i + \rho_0 \mathbf{e}_i + L\mathbf{w}_i = \mathbf{0}$, $i = 1, \cdots, 3$, where ρ_0 is the actuation length at home position. In practical application, all three P joints are usually set to be half actuated ($\rho_0 = \frac{\rho_{max}}{2}$) when the mechanism is at home position. Note that $\mathbf{e}_i$, $i = 1, \cdots, 3$ are unit vectors and they provide three equality constraints for design parameters. Therefore, totally there are 16 independent design parameters.

Assume $\mathbf{d}_i = [d_{i1}\ d_{i2}\ d_{i3}]^T$ and $\mathbf{e}_i = [e_{i1}\ e_{i2}\ e_{i3}]^T$, for $i = 1, \cdots, 3$. Combining the objective and constraints together, the optimal design problem of a 3-PP_a^* parallel mechanism is formulated as follows.

Problem 1: Optimal design of a 3-PP_a^* parallel mechanism

Find a set of optimal design parameters α such that

$$\begin{aligned} \max_{\alpha} \quad & \Phi = l \\ \text{subject to} \quad & \kappa(J(X, \rho, \alpha)) \geq 0.2; \\ & 0 \leq \rho_i(X, \alpha) \leq \rho_{max}; \\ & 0 \leq \text{Angle}(\mathbf{w}_j, \mathbf{w}_j^0) \leq 30^\text{o}; \\ & L + \rho_{max} = 1; \\ & d_{kl},\ e_{kl} \in [-1, 1], \\ & x_c,\ y_c,\ z_c \in [-0.5, 0.5], L \in [0, 1] \end{aligned}$$

for all $X \in W$, $i, j, k, l = 1, \cdots, 3$. □

By applying the controlled random search (CRS) algorithm [14], optimal design parameters and the corresponding maximal side length are obtained, as shown in Table I and II. From Table I, $\mathbf{e}_1 \cdot \mathbf{e}_2 = -0.0643$, $\mathbf{e}_1 \cdot \mathbf{e}_3 = 0.0737$, $\mathbf{e}_2 \cdot \mathbf{e}_3 = 0.0097$. They all tend to zeroes, which implies that $\mathbf{e}_i$, $i = 1, \cdots, 3$ nearly perpendicular mutually. We may

TABLE I

OPTIMAL FOOTPRINTS AND LINEAR JOINT AXES

$\mathbf{d}_1$	$(-0.7893,\ -0.0358,\ -0.0334)^T$	$\mathbf{e}_1$	$(0.9998,\ 0.0185,\ 0.0042)^T$
$\mathbf{d}_2$	$(0.0067,\ -0.7881,\ -0.0587)^T$	$\mathbf{e}_2$	$(-0.0830,\ 0.9938,\ 0.0736)^T$
$\mathbf{d}_3$	$(-0.0574,\ -0.0047,\ -0.7884)^T$	$\mathbf{e}_3$	$(0.0706,\ -0.05814,\ 0.9958)^T$

TABLE II

OPTIMAL CUBIC WORKSPACE CENTER AND GEOMETRIC PARAMETERS

x_c	y_c	z_c	L	ρ_{max}	$\Phi^* = l^*$
-0.0279	-0.0279	-0.0279	0.5822	0.4178	0.1792

TABLE III

OPTIMAL FOOTPRINTS AND THE FIXED LINEAR JOINT AXES

$\mathbf{d}_1$	$(-0.7884,\ -0.0278,\ -0.0278)^T$	$\mathbf{e}_1$	$(1,\ 0,\ 0)^T$
$\mathbf{d}_2$	$(-0.0279,\ -0.7884,\ -0.0279)^T$	$\mathbf{e}_2$	$(0,\ 1,\ 0)^T$
$\mathbf{d}_3$	$(-0.0279,\ -0.0278,\ -0.7884)^T$	$\mathbf{e}_3$	$(0,\ 0,\ 1)^T$

conjecture that the true global optimum is obtained from the mechanism that has mutually perpendicular axes of fixed prismatic joints. Therefore, further optimizations are carried out with fixed linear joint axes $\mathbf{e}_1 = (1\ 0\ 0)^T$, $\mathbf{e}_2 = (0\ 1\ 0)^T$, $\mathbf{e}_3 = (0\ 0\ 1)^T$. Under this circumstance, optimization results are obtained, as shown in Table III and IV. From Table IV, the objective, the maximum half side length of the cubic effective workspace is a little bit larger than that of the previous optimization. We may then conclude that the best mechanism is the one whose base-fixed prismatic joint axes are mutually perpendicular. Furthermore, it can be verified that the three axes of fixed prismatic joints intersect at a common point.

The side length of the maximal effective regular workspace is about $2 \times 0.18 = 0.36$. The stroke ρ_{max} is about 0.42. Using the optimal design parameters, we can verify that dexterity performance reaches its best, $\kappa = 1$, at the center $(x_c, y_c, z_c) = (-0.02785, -0.02785, -0.02785)$. At this position, each spatial parallelogram is parallel to its corresponding linear joint axis. As a result, all subchains form straight lines and become perpendicular to each other. Therefore, the resulting design is an isotropic mechanism since its workspace contains an isotropic configuration. This is a preferable property in mechanism design [15][16][17]. Fig. 4 shows a CAD model of the resulting mechanism. It is architecturally similar to the Orthoglide, as shown in Fig. 5-(a). They both consist of three orthogonally arranged, identical subchains. But topologically they are quite different. For the Orthoglide, each subchain is in a PRP_aR topology, while our resulting mechanism has subchains of PP_a^* topology. The Linapod, as shown in Fig. 5-(b), is a tripod based parallel machine with the same 3-PP_a^* topology as the resulting mechanism. The resulting mechanism thus has characteristics of both the Orthoglide and the tripod. The resulting mechanism is therefore named the Orthopod.

Fig. 6-(a) shows a scaled schematic of the Orthopod

TABLE IV

OPTIMAL CUBIC WORKSPACE CENTER AND GEOMETRIC PARAMETERS IN THE CASE OF FIXED LINEAR JOINT AXES

x_c	y_c	z_c	L	ρ_{max}	$\Phi^* = l^*$
-0.0279	-0.0279	-0.0279	0.5795	0.4206	0.1803

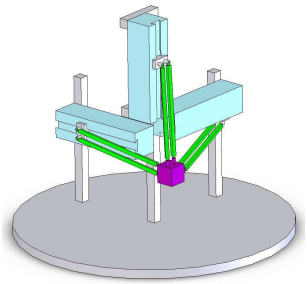

Fig. 4. A CAD model of the resulting mechanism

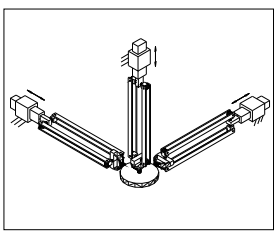

(a)

(b)

Fig. 5. (a)A CAD model of the Orthoglide; (b)The Linapod developed by ISW.

at its home configuration. It is interesting to note that at home configuration, the parallelogram is *not* parallel to its corresponding linear joint axis. In other words, the home configuration is *not* the isotropic configuration. Using the subchain 1 for example, Fig. 6-(b) shows its pose at home configuration. The parallelogram 1 makes an angle $\theta_1 \approx 3.9^{\circ}$ with x-axis ($= \mathbf{e}_1$). In the yz plane, the parallelogram 1 makes an angle $\theta_2 = 45^{\circ}$ with z-axis. It is also the case for the other two subchains with their respectively corresponding axes. This phenomenon is induced because, as shown in Fig. 7-(b), 8-(b), 9-(b), the dexterity performance is not centrally symmetric about the isotropic point.

Fig. 7-(a), 8-(a), and 9-(a) show workspace cross sections at $z = z_c + l^*$, $z = z_c$, and $z = z_c - l^*$. The shadowed squares represent cross sections of maximal effective cubic workspace. In all three figures, the shadowed squares touch the workspace boundary. It shows that the workspace constraints become active. In Fig. 7-(b), 8-(b), and 9-(b), contour plots of dexterity index are given at cross sections $z = z_c + l^*$, $z = z_c$, and $z = z_c - l^*$ of the maximal effective cubic workspace. Using resulting geometry for the Orthopod, we can find the minimum value of the dexterity index is 0.2281, which is obviously larger than the given threshold, $\gamma = 0.2$. This shows that the dexterity constraint is inactive.

Using the optimal architecture, a prototype machine of the Orthopod is manufactured as shown in Fig. 10. It exhibits good positioning accuracy with acceleration from 0 to $4g$. Further investigations are conducting on the prototype.

IV. CONCLUSION

Inspired by the successful application of the parallelogram in Delta robot and its variants, we investigated the spatial parallelogram P_a^* in detail. It was shown that a parallel

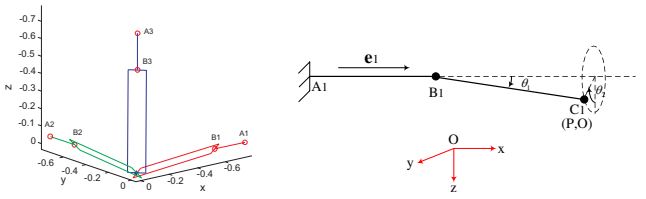

(a) (b)

Fig. 6. (a) A scaled schematic of the resulting mechanism at its home configuration; and (b) A schematic of subchain 1 at its home configuration.

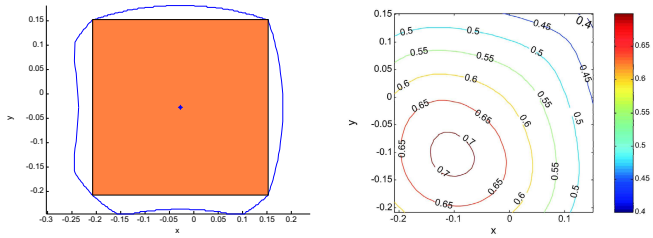

(a) (b)

Fig. 7. (a) Workspace cross section at $z = z_c + l^*$; (b) Contour plot of dexterity index at cross section $z = z_c + l^*$.

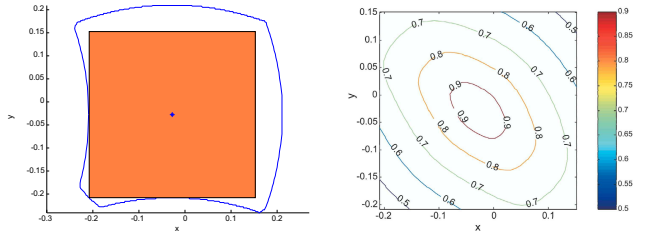

(a) (b)

Fig. 8. (a) Workspace cross section at $z = z_c$; (b) Contour plot of dexterity index at cross section $z = z_c$.

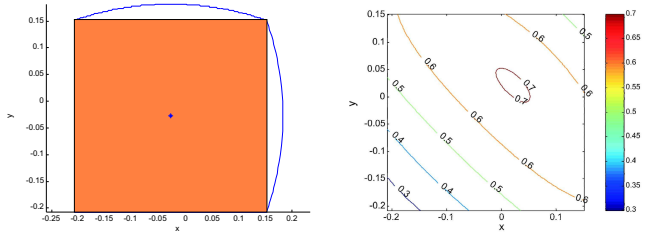

(a) (b)

Fig. 9. (a) Workspace cross section at $z = z_c - l^*$; (b) Contour plot of dexterity index at cross section $z = z_c - l^*$.

Fig. 10. The Orthopod prototype

mechanism consisting of three or more PP_a^* subchains generically undergoes 3-DoF purely translational motion. In order to find the architecture best suit our task, we optimally design a 3-PP_a^* parallel mechanism including its architecture and geometry parameters. The Orthopod, whose axes of prismatic joints are mutually perpendicular and intersect at a common point, was thus obtained as the optimum. A prototype machine of the Orthopod was manufactured and constructed.

REFERENCES

[1] D. Stewart. A platform with six degrees of freedom. In *Proc. Inst. Mech. Eng., vol. 180, London, England*, pages 371–386, 1965.

[2] V.E. Gough and S.G. Whitehall. Universal tyre test machine. In *Proc. 9th Int. Tech. Congress, F.I.S.I.T.A.*, page 177, 1962.

[3] R. Clavel. Delta, a fast robot with parallel geometry. In *Proc. 18th International Symposium on Industrial Robots*, pages 91–100, 1988.

[4] D. Chablat and P. Wenger. Architecture optimization of a 3-dof translational parallel mechanism for machining applications, the orthoglide. *IEEE Transactions on Robotics and Automation*, 19(3):403–410, 2003.

[5] L. W. Tsai. Kinematics of a three-dof platform with three extensible limbs. *Recent Advances in Robot Kinematics: Analysis and Control, J. Lenaric and V. Parenti-Castelli, Eds. Norwell, MA: Kluwer*, pages 49–58, 1996.

[6] R. Di Gregorio and V. Parenti-Castelli. A translational 3-DOF parallel manipulator. *Recent Advances in Robot Kinematics: Analysis and Control, J. Lenaric and V. Parenti-Castelli, Eds. Norwell, MA: Kluwer*, pages 401–410, 1998.

[7] Y.J. Lou and Z.X. Li. A novel 3-dof purely translational parallel mechanism. In *Proceedings of IEEE/RSJ International Conference on Intelligent Robots and Systems*, 2006.

[8] J. Meng, G. F. Liu, and Z. X. Li. A geometric theory for synthesis and analysis of sub-6 DoF parallel manipulators. In *Proceedings of IEEE International Conference on Robotics and Automation*, pages 2938 – 2943, 2005.

[9] J. Meng, G.F. Liu, and Z.X. Li. A geometric theory for synthesis and analysis of sub-6 DoF parallel manipulators. *Submitted to the IEEE Transactions on Robotics*, 2006.

[10] F. Gao, W.M. Li, X.C. Zhao, Z.L. Jin, and H. Zhao. New kinematic stuctures for 2-, 3-, 4-, and 5-dof parallel manipulator design. *Mechanism and Machine Theory*, 37(11):1395–1411, 2002.

[11] R.E. Stamper, L.W. Tsai, and G.C. Walsh. Optimization of a three dof translational platform for well-conditioned workspace. In *Proceedings of IEEE International Conference on Robotics and Automation*, pages 3250–3255, 1997.

[12] D. Chablat, P. Wenger, F. Majou, and J-P. Merlet. An interval analysis based study for the design and the comparison of three-degrees-of-freedom parallel kinematic machines. *The International Journal of Robotics Research*, 23(6):615–624, 2004.

[13] A. Kosinka, M. Galicki, and K. Kedzior. Designing and optimization of parameters of delta-4 parallel manipulator for a given workspace. *Journal of Robotic Systems*, 20(9):539–548, 2003.

[14] Y.J. Lou, G.F. Liu, N. Chen, and Z.X. Li. Optimal design of parallel manipulators for maximum effective regular workspace. In *Proceedings of IEEE/RSJ International Conference on Intelligent Robots and Systems*, pages 1208–1213, 2005.

[15] J. Angeles. Kinematic isotropy in humans and machines. In *Proceedings of IFToMM 9th World Congress on Theory of Machines and Mechanisms*, pages XLII–XLIX, 1995.

[16] K.E. Zanganeh and J. Angeles. Kinematic isotropy and the optimum design of parallel manipulators. *The International Journal of Robotics Research*, 16(2):185–197, 1997.

[17] A. Fattah and A.M.H. Ghasemi. Isotropic design of spatial parallel manipulators. *The International Journal of Robotics Research*, 21(9):811–824, 2002.